IEEE Access
Multidisciplinary | Rapid Review | Open Access Journal

Received September 6, 2019, accepted September 27, 2019, date of publication October 2, 2019, date of current version October 24, 2019.

Digital Object Identifier 10.1109/ACCESS.2019.2945195

Study on Voltage Stability and Control Strategy of Grid-Connected Wind Farm

XINYU LIU, GUOFANG WU, AND XIANWEI LI
School of Electric Power, North China University of Water Resource and Electric Power, Zhengzhou 450011, China

Corresponding author: Xinyu Liu (lxy22101@163.com)

This work was supported in part by the Henan Science and Technology Research Project under Grant 162102210078, in part by the Henan Key Youth Teacher Research Project under Grant 2016GGJS-074, and in part by the Henan Provincial Department of Education Science and Technology Research Key Project under Grant 14B413005.

ABSTRACT Aiming at the Low voltage ride through capability of doubly-fed wind farm when it is merged into a weak grid, this paper researches the theory of rotor excitation control and proposed an additional control model of DFIG grid-connected rotor flux based on structure decentralization theory. In this model, the Low voltage ride through capability of the doubly-fed wind farm is enhanced by designing the d-axis and q-axis adaptive terminal sliding mode controllers for the synchronous rotating coordinate system. Simulation results show that the proposed control model not only can better realize the rapid regulation of reactive power of doubly-fed wind farms, but also improve the ability of the system to resist grid voltage fluctuations, and improve the transient stability of power systems. It has certain theoretical significance and practical application value.

INDEX TERMS Doubly-fed, grid-connected, structural decentralization, adaptive.

I. INTRODUCTION

Wind power generation is a renewable energy generation method. It has many advantages. It can not only reduce environmental pollution, but also alleviate the energy crisis. Its role in the implementation of low-carbon development strategy is increasingly prominent [1], [2]. With the increase of China's wind power installed capacity, the contradiction between wind power grid connection and power system transient stability has become increasingly prominent [3]–[6]. This contradiction is mainly manifested in voltage stability at the busbar of the wind farm when the grid is faulty. The reason for the drastic change of transient voltage is lack of fast regulation capability of transient reactive power in wind farms, which may lead to the occurrence of grid voltage cascading accidents and bring greater security risks to the grid-connected operation of wind farms. In response to the stability of wind power grid connection, many countries have specified the technical requirements for grid connection of large wind farms [7], [8]. One of the requirements is that the system needs to quickly send reactive power to regulate the voltage in the event of a grid failure.

The associate editor coordinating the review of this manuscript and approving it for publication was Canbing Li.

At present, scholars have done a lot of work on wind power generation, and have made some achievements [9]–[14]. Literature [15] discusses an optimal control method. It is a control method based on energy function used in DFIG-flywheel energy storage architecture. This method can mitigate oscillations and is very effective in increasing wind energy penetration. Literature [16] proposed a method to improve the low voltage ride through capability. In this method, the stator and rotor electromotive force models in the wind turbine are designed, and the new stator-damping resistor unit (SDRU) and rotor current control (RCC) are combined with the stator and rotor electromotive force models. Use this control method to get a stable system in a short time. Literature [17] discusses the hybrid ESS. This document analyzes real-time simulation of a wind turbine generator coupled with a battery supercapacitor energy storage system. Simulation analysis shows that the hybrid ESS has lower cost, longer usage time and higher efficiency. Reference [18] discusses the application of Demagnetization Current Controller (DCC) to DFIG. Simulation results show that this method can make the system stable in a short time. Literature [19] introduced an independent hybrid power generation system and analyzed its dynamic behavior and simulation results. By analyzing the optimal size and economy, the cost of the system is reduced. The system reduces environmental pollution and extracts

maximum power from the wind energy conversion system. Literature [20] introduced a control method to enhance the capability of Fault ride-through (FRT). It studies the application of positive-negative-sequence dynamic modeling (PNSDM) and supercapacitor in DFIG-based wind farms. The simulation results show that it effectively improves the FRT ability of the system. Reference [21] proposes a nonlinear control method that uses this method to control the grid-side converter of the DFIG to enhance low-voltage ride-through capability. Simulation results show that the control method has good control effect. Reference [22] discusses a method for improving low voltage ride through. By designing and comparing the passive Low voltage Ride Through (LVRT) capability method and the active LVRT capability method, it is found that the low voltage ride-through capability is improved when the active LVRT is combined with the DFIG model. Reference [23] proposes a method to improve the voltage ride-through capability, which is accomplished by joint use of the rotor-side converter control and a three-phase stator damping resistor (SDR) placed in series with the stator windings. The control method reduces the peak of the rotor inrush current, the electromagnetic torque and the DFIG transient response, and achieves a good control effect.

According to the analysis of the above documents, domestic and foreign scholars have less research on the rapidity of reactive power regulation about DFIG voltage stability. However, the millisecond-level output reactive power is critical to improving low voltage ride through capability. This paper proposes an adaptive terminal sliding mode additional control strategy for rotor flux linkage by the basic grid-connected operation model of DFIG. During a grid fault, the DFIG using this control strategy can quickly generate reactive power and reduce the bus voltage, thereby improving low voltage ride through capability.

II. DFIG STRUCTURE DECENTRALIZED DYNAMIC MATHEMATICAL MODEL

After using the coordinate transformation matrix for coordinate transformation, we can get the voltage equation and flux linkage equation in the two-phase synchronous rotating coordinate system as shown below.

The stator voltage equations of the d and q axes of the doubly-fed induction generator are as follows,

$$\begin{cases} u_{ds} = R_s i_{ds} - \omega_1 \Psi_{qs} + \dfrac{d\Psi_{ds}}{dt} \\ u_{qs} = R_s i_{qs} + \omega_1 \Psi_{ds} + \dfrac{d\Psi_{qs}}{dt} \end{cases} \tag{1}$$

The rotor voltage equations of the d and q axes of the doubly-fed induction generator are as follows,

$$\begin{cases} u_{dr} = R_r i_{dr} - \omega_s \Psi_{qr} + \dfrac{d\Psi_{dr}}{dt} \\ u_{qr} = R_r i_{qr} + \omega_s \Psi_{dr} + \dfrac{d\Psi_{qr}}{dt} \end{cases} \tag{2}$$

where u_{ds} and u_{qs} are the d-axis and q-axis components of the stator voltage of the doubly fed induction generator, u_{dr} and u_{qr} are the d-axis and q-axis rotor voltage of the doubly fed induction generator, u_{qr} are the q-axis rotor voltage of the doubly fed induction generator, i_{ds} and i_{qs} are the d-axis and q-axis stator current, i_{dr} and i_{qr} are the d-axis and q-axis rotor current of the doubly fed induction generator, Ψ_{ds} and Ψ_{qs} are the d-axis and q-axis stator magnetic linkage of the doubly fed induction generator, Ψ_{dr} and Ψ_{qr} are the d-axis and q-axis rotor magnetic linkage, ω_r is rotational speed of doubly-fed induction generator rotor, ω_1 is synchronous speed, $\omega_s = \omega_1 - \omega_r$ is the rotational speed of a two-phase synchronous rotating coordinate system relative to the rotor.

The stator flux linkage equation for the d and q axes of a doubly fed induction generator is shown below,

$$\begin{cases} \Psi_{ds} = L_s i_{ds} + L_m i_{dr} \\ \Psi_{qs} = L_s i_{qs} + L_m i_{qr} \end{cases} \tag{3}$$

The rotor flux linkage equation for the d and q axes of a doubly fed induction generator is shown below,

$$\begin{cases} \Psi_{dr} = L_m i_{ds} + L_r i_{dr} \\ \Psi_{qr} = L_m i_{qs} + L_r i_{qr} \end{cases} \tag{4}$$

where L_m is the mutual inductance between the stator and rotor coaxial equivalent windings of the doubly-fed induction generator under the two-phase synchronous rotating coordinate system. L_s is the self-inductance of the stator equivalent two-phase winding of the doubly-fed induction generator under the two-phase synchronous rotating coordinate system. L_r is the self-inductance of the equivalent two-phase winding under two-phase synchronous rotating coordinate system.

The torque equation of the doubly-fed wind turbine is as follows,

$$T_e = n_p L_m (i_{qs} i_{dr} - i_{ds} i_{qr}) \tag{5}$$

The equation of motion for a doubly-fed induction generator is shown below,

$$T_m = T_e + \frac{J}{n_p} \frac{d\omega}{dt} \tag{6}$$

The stator active power and reactive power equations are as follows,

$$\begin{cases} P_s = u_{ds} i_{ds} + u_{qs} i_{qs} \\ Q_s = u_{qs} i_{ds} - u_{ds} i_{qs} \end{cases} \tag{7}$$

where P_s and Q_s are the stator active and reactive power.

When the grid voltage is symmetrically operated, the stator flux linkage is oriented on the d-axis of the d-q coordinate system. And the magnetic fluxes on the d and q axes are $\Psi_{ds} = \Psi_s$, $\Psi_{qs} = 0$. The stator voltage of the DFIG is equal to the induced electromotive force, that is, $u_{ds} = 0$, $u_{qs} = u_s$; u_{qs} is the amplitude of the vector of the stator voltage. When the stator is incorporated into the ideal grid, u_{qs} is equal to amplitude of the grid voltage. The resistance of stator winding is much smaller than the reactance of stator winding, so the

influence of stator resistance can be ignored. Get the equation shown below,

$$\begin{cases} \psi_{ds} = \dfrac{u_{qs}}{\omega_1} = \dfrac{u_s}{\omega_1} \\ \dfrac{d\Psi_{ds}}{dt} = 0 \end{cases} \tag{8}$$

$$\begin{cases} i_{ds} = \dfrac{L_m i_{dr} - \psi_{ds}}{L_s} \\ i_{qs} = \dfrac{L_m i_{qr}}{L_s} \end{cases} \tag{9}$$

DFIG is unstable when the grid fails. Have the following equation of state, $\frac{d\Psi_{ds}}{dt} \neq 0$.

From the above, we can get the following equation,

$$\begin{cases} \dfrac{d\Psi_{dr}}{dt} = -\dfrac{R_r L_s}{L_m^2 - L_r L_s}\psi_{dr} + \omega_s \psi_{qr} \\ \qquad\qquad -\dfrac{R_r L_m u_s}{\omega_1 (L_m^2 - L_r L_s)} + u_{dr} \\ \dfrac{d\Psi_{qr}}{dt} = -\dfrac{R_r L_s}{L_m^2 - L_r L_s}\psi_{qr} - \omega_s \psi_{dr} + u_{qr} \end{cases} \tag{10}$$

Then the active output power equation and reactive power output equation of the stator are as follows,

$$\begin{cases} P_s = \dfrac{u_s L_m}{L_s} i_{qr} = \dfrac{u_s L_m}{L_m^2 - L_r L_s}\psi_{qr} \\ Q_s = \dfrac{u_s L_m}{L_s} i_{dr} - \dfrac{u_s}{L_s}\psi_{ds} \\ \quad = \dfrac{u_s L_m}{L_m^2 - L_r L_s}\psi_{dr} \\ \qquad + \dfrac{(L_m^2 - L_s L_m + L_r L_s^2) u_s}{L_s (L_m^2 - L_r L_s)}\psi_{ds} \end{cases} \tag{11}$$

The mathematical model of the grid-side converter is shown below,

$$\begin{cases} L\dfrac{di_{gd}}{dt} = -Ri_{gd} + \omega L i_{gq} + u_{gd} - v_{gd} \\ L\dfrac{di_{gq}}{dt} = -Ri_{gq} - \omega L i_{gd} + u_{gq} - v_{gq} \\ C\dfrac{du_{dc}}{dt} = \left(S_d i_{gd} + S_q i_{gq}\right) - i_L \end{cases} \tag{12}$$

where u_{gd} and u_{gq} are the d-axis and q-axis components of the power grid voltage; v_{gd} and v_{gq} are the d-axis and q-axis components of the output voltage vector of the three-phase VSR AC side; i_{gd} and i_{gq} are the d-axis and q-axis components of three-phase VSR input current vector; S_d and S_q are the d-axis and q-axis components of the switching function; ω is angular velocity of the grid voltage; L is inductance of the line reactor; R is line resistance; C is DC bus capacitor; i_L is load current on the DC side.

When the d-axis of the synchronous rotating coordinate system is oriented in the direction of the grid voltage vector, then, $u_{gd} = u_g$,$u_{gq} = 0$.

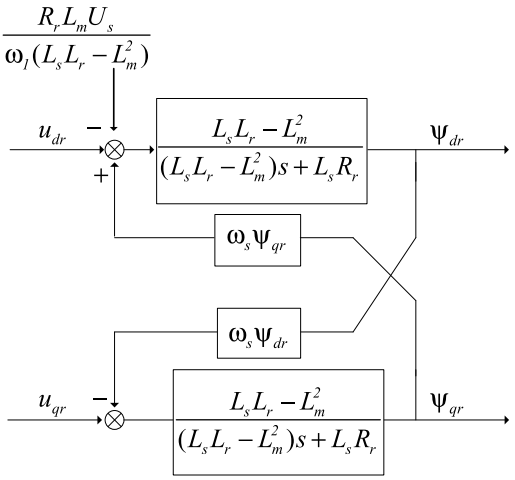

FIGURE 1. Structure diagram of relationship between rotor applied voltage and rotor flux linkage of DFIG.

Then you can get the following equation,

$$\begin{cases} L\dfrac{di_{gd}}{dt} = -Ri_{gd} + \omega L i_{gq} + u_g - v_{gd} \\ L\dfrac{di_{gq}}{dt} = -Ri_{gq} - \omega L i_{gd} - v_{gq} \\ C\dfrac{du_{dc}}{dt} = (S_d i_{gd} + S_q i_{gq}) - i_{load} \end{cases} \tag{13}$$

In the part of the grid-side converter output to the grid, the active output power and reactive power output equation are as follows,

$$\begin{cases} P_g = -\dfrac{3}{2} u_g i_{gd} \\ Q_g = \dfrac{3}{2} u_g i_{gq} \end{cases} \tag{14}$$

where P_g denotes active output power, Q_g denotes reactive output power, u_g is grid electromotive force.

III. DFIG ADDITIONAL ROTOR MAGNETIC LINKAGE CONTROL DESIGN

According to equation (10), the relationship between the applied voltage of the variable-frequency drive on the rotor and the rotor magnetic linkage during power generation operation is shown in Figure 1.

As can be seen from Figure 1, when the system starts grid-connected operation, the input to the control system is the rotor voltage, which are u_{dr} and u_{qr}, and the output is the rotor flux linkage, which are ψ_{dr} and ψ_{qr}. Therefore, by designing the controller of the DFIG rotor flux system, the control of the rotor flux linkage of the generator is realized.

In order to make the DFIG rotor flux component better deal with the interference of the grid fault and achieve strong robustness, the sliding mode variable structure control strategy can be introduced. Rewrite equation (10) to the following state space expression,

$$\dot{Z} = AZ + BU + F \tag{15}$$

$$A = \begin{bmatrix} -\frac{L_s R_r}{L_s L_r - L_m^2} & \omega_s \\ -\frac{L_s R_r}{L_s L_r - L_m^2} & -\omega_s \end{bmatrix} \quad (15-1)$$

$$B = \begin{bmatrix} 1 & 0 \\ 0 & 1 \end{bmatrix} \quad (15-2)$$

$$F = \begin{bmatrix} f \\ 0 \end{bmatrix} \quad (15-3)$$

$$f = -\frac{R_r L_m U_s}{\omega_1 (L_s L_r - L_m^2)} \quad (15-4)$$

where, F is the disturbance to the system when the grid fails, $z = \begin{bmatrix} z_{11} \\ z_{21} \end{bmatrix}$ is state variable, $U = \begin{bmatrix} z_{10} \\ z_{20} \end{bmatrix}$ is control input, z_{11} is the d-axis rotor magnetic linkage, which is ψ_{dr}; z_{21} is the q-axis rotor magnetic linkage, which is ψ_{qr}; z_{20} is the q-axis rotor current control signal, which is u_{qr}; z_{10} is the d-axis rotor current control signal, which is u_{dr}.

Know the following equation,

$$rank\,[B \quad F] = rank\,[B] = 2 \quad (16)$$

It can be seen from equation (16) that the doubly-fed wind power generation system controlled by the sliding mode is relatively robust, and it is basically free from external interference. Therefore, using a sliding mode to design a suitable controller can effectively reduce the interference caused by grid fluctuations on the doubly-fed wind power generation system.

Let the error of the q-axis component of the rotor flux linkage and its given value be $e_d = z_{11}^* - z_{11}$, and use it as the state variable of the system, then the error state space equation of the d-axis component of the rotor flux linkage can be obtained from the expression (10). The equation is as follows,

$$\dot{e}_d = -\frac{R_r L_s}{L_m^2 - L_r L_s} e_d - \omega_s z_{21} - z_{10} + F_d \quad (17)$$

$$F_d = \left(\frac{L_s R_r}{L_m^2 - L_s L_r} z_{11}^* + f\right) \quad (17-1)$$

where F_d represents the interference caused by the fluctuation of the power grid.

In summary, the proposed integral sliding surface is as follows,

$$s_d = k_{pd} e_d + k_{id} \int_0^t e_d^{p/q} d\tau \quad (18)$$

where k_{pd} and k_{id} are proportionality coefficient and integral coefficient, k_{pd} and k_{id} are both larger than zero.

The proportional term makes the system response faster and reduces the reaction time. The integral term eliminates the static error of the system and improves the stability. It can be seen from the expression that on the PI integral sliding mode hypersurface, the dynamic characteristics of the sliding surface depend on the values of k_{pd} and k_{id}.

For the integral sliding surface proposed above, the controlled system often fails to achieve good control effect, and its anti-interference ability can not be guaranteed. The reason is that in actual control, the upper bound of parameter F_d is uncertain. That is to say, in the case of strong interference in the system, in order to maintain the robustness of the system in a strong state, it is necessary to increase the value of the switching gain η_d, which may cause an unstable state of severe jitter in the system. In order to solve such system defects, the switching gain needs to be improved, and a sliding mode variable structure controller with adaptive switching gain is designed. The improved switching gain expression is as follows,

$$\eta_d'(t) = (1 + \mu(s) e_d^{\lambda_d \mu(s) t}) \eta_d \quad (19)$$

$$\mu(s_d) = \mathrm{sgn}(s_d)\mathrm{sgn}(s_d') \quad (19-1)$$

$$s_d'(t) = s_d(t + \tau) \quad (19-2)$$

where τ is the delay time constant and $0 < \lambda_d < 1$.

When the system moves away from the sliding surface, the switching gain of the system will increase rapidly in the manner of $\eta_d'(t)=(1+e_d^{\lambda_d t})\eta_d$. When the system moves across the sliding surface, the switching gain of the system will decrease rapidly in the manner of $\eta_d'(t)=(1-e_d^{\lambda_d t})\eta_d$.

By analyzing the integral terminal sliding surface shown in equation (16), it is known that if the doubly-fed wind turbine system satisfies the condition of the generalized perturbation term $|F_d| < k_d$(k_d is the constant and $k_d > 0$), then the following control law can be obtained under the adaptive switching gain η_d'.

$$z_{10} = -\frac{R_r L_s}{L_m^2 - L_r L_s} e_d - \omega_s z_{21} + \frac{k_{id}}{k_{pd}} e_d^{p/q} + \eta_d' \mathrm{sgn}(s_d) \quad (20)$$

It can be seen from the above equation that the error between the d-axis flux linkage of DFIG and the given value tends to zero in a limited time, and the system robustness does not change.

Next, prove the above law:

By the model of the integral sliding surface, the integral term is initialized as follows:

$$\int_{-\infty}^{0} e_d^{p/q} d\tau = -\frac{k_{pq}}{k_{iq}} e_{d0} \quad (21)$$

where e_{d0} denotes deviation of the initial time of the system.

When t = 0, put the formula (21) into the formula (18), and get,

$$s_d(0) = k_{pd} e_{d0} + k_{id} \int_{-\infty}^{t} e_d^{p/q}(\tau) d\tau = k_{pd} e_{d0} - k_{id} \frac{k_{pd}}{k_{id}} e_{d0} = 0 \quad (22)$$

Equation (22) shows that by selecting the appropriate initial value to make $s_d(0) = 0$, the initial state of the system can fall on the sliding surface, which enhances the anti-interference ability of the system.

According to equation (14) that when the system reaches the sliding surface, there is $\dot{s}_d = s_d = 0$, there are equations as follows as,

$$\dot{e}_d = -\frac{k_{id}}{k_{pd}} e_d^{p/q} \quad (23)$$

The following equation can be obtained from equation (17),

$$\dot{e}_d \frac{1}{\frac{k_{id}}{k_{pd}} e_d^{p/q}} = -1 \tag{24}$$

Integrate the left and right sides of the above formula,

$$\int_{e_d}^{0} \frac{1}{\frac{k_{id}}{k_{pd}} e_d^{p/q}} de_d = -\int_{0}^{\Delta td} dt \tag{25}$$

The equation for solving (25) is as follows,

$$\Delta t_d = \frac{q k_{pd}}{k_{id}(q-p)} e_d^{1-\frac{p}{q}} \tag{26}$$

It can be proved from the above formula that the error of the d-axis flux linkage component of the doubly-fed induction wind turbine gradually approaches zero in the Δt_d time.

It is pointed out above that the switching gain $\eta_d^{'}$ adopts an adaptive control method, but the initial value is determined in two cases, namely, $\eta_d^{'} > k_d$ and $\eta_d^{'} < k_d$. The stability of the system in two cases is discussed below:

When $\eta_d^{'} < k_d$ and $\eta_d^{'} > |F_d|$, the Lyapunov function is selected as $V = \frac{1}{2}s_d^2$, and then,

$$\begin{aligned}
\dot{V} &= s_d \dot{s}_d \\
&= s_d[k_{pd}(-\frac{R_r L_s}{L_m^2 - L_r L_s} e_d - \omega_s z_{21} - z_{10} + F_d) + k_{id} e_d^{p/q}] \\
&= s_d(-k_{pd}\frac{R_r L_s}{L_m^2 - L_r L_s} e_d - k_{pd}\omega_s z_{21} + k_{pd}\frac{R_r L_s}{L_m^2 - L_r L_s} e_d \\
&\quad + k_{pd}\omega_s z_{21} - k_{id} e_d^{p/q} - \eta_d' \mathrm{sgn}(s_d) + k_{pd} F_d + k_{id} e_d^{p/q}) \\
&= s_d(-\eta_d' \mathrm{sgn}(s_d) + F_d) \le (-\eta_d' |s_d| + |F_d||s_d|) \\
&\quad \le -|s_d|(\eta_d' - k_d) < 0
\end{aligned} \tag{27}$$

It can be seen from Equation (27) that the condition that the system reaches the sliding surface is always satisfied, which proves that the system is stable in terms of robustness.

When $\eta_d^{'} < k_d$ and $\eta_d^{'} < |F_d|$, the Lyapunov function is selected as $V = \frac{1}{2}s_d^2$, and the following equation is obtained,

$$\begin{aligned}
\dot{V} &= s_d \dot{s}_d \\
&= s_d[k_{pd}(-\frac{R_r L_s}{L_m^2 - L_r L_s} e_d - \omega_s z_{21} - z_{10} + F_d) + k_{id} e_d^{p/q}] \\
&= s_d(-k_{pd}\frac{R_r L_s}{L_m^2 - L_r L_s} e_d - k_{pd}\omega_s z_{21} + k_{pd}\frac{R_r L_s}{L_m^2 - L_r L_s} e_d \\
&\quad + k_{pd}\omega_s z_{21} - k_{id} e_d^{p/q} - \eta_d' \mathrm{sgn}(s_d) + k_{pd} F_d + k_{id} e_d^{p/q}) \\
&= s_d(-\eta_d' \mathrm{sgn}(s_d) + F_d) \le (-\eta_d' |s_d| + |F_d||s_d|) \\
&\le -|s_d|(\eta_d' - |F_d|)
\end{aligned} \tag{28}$$

According to $\eta_d^{'} < |F_d|$, $-|s_d|(\eta_d' - |F_d|) > 0$ can be launched, and it can be seen that the system will be start moving away from the sliding surface. However, under the improved control method, the adaptive switching gain will increase rapidly with time. Due to the boundedness of $|F_d|$, the situation of $\eta_d^{'} > |F_d|$ will appear. When $\eta_d^{'} > |F_d|$, there is $\dot{V} = s_d \dot{s}_d < 0$. At this point, the condition that the system reaches the sliding surface is satisfied.

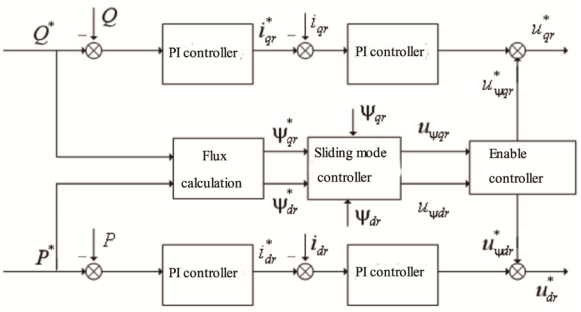

FIGURE 2. Block diagram of rotor flux linkage sliding mode control based on DFIG.

The control method described above controls the system to move near the sliding surface. As time changes, the amplitude of η_d' will gradually decrease, which will gradually reach the sliding surface of the system, thus making the system more stable.

Similarly, the q-axis magnetic linkage component control law is the following equation,

$$z_{20} = -\frac{R_r L_s}{L_m^2 - L_r L_s} e_q - \omega_s z_{11} + \frac{k_{iq}}{k_{pq}} e_q^{p/q} + \eta_q' \mathrm{sgn}(s_q) \tag{29}$$

Through the design of the control method, the block diagram of rotor flux linkage sliding mode control based on DFIG is designed. The control block diagram is shown in Figure 2. The expression of the Enable control is as follows.

$$\begin{cases} u_{\psi dr}^* = u_{\psi dr} \mathrm{sgn}(\left|\psi_{dr}^* - \psi_{dr}\right|) \\ u_{\psi qr}^* = u_{\psi qr} \mathrm{sgn}(\left|\psi_{qr}^* - \psi_{qr}\right|) \end{cases} \tag{30}$$

It can be seen from Fig. 2 that according to the given values of active and reactive power and equation, the rotor flux component command values ψ_{qr}^* and ψ_{dr}^* are calculated, and the flux linkage feedback values ψ_{qr} and ψ_{dr} are calculated through the real-time calculation of the flux linkage. Then the controller outputs the control signal of the inverter, which are $u_{\psi_{dr}}^*$ and $u_{\psi_{qr}}^*$. The flux linkage additional control signal acts during the disturbance of the grid. Due to the strong robustness of the flux-chain sliding mode controller, it can suppress sharp changes in the power angle of the DFIG during large disturbances. Therefore, it is possible to improve voltage drop and rotor overcurrent.

IV. DFIG GRID-CONNECTED OPERATION OPTIMIZATION CONTROL EXAMPLE SIMULATION

This paper presents a DFIG additional rotor flux linkage adaptive terminal sliding mode control strategy. In order to observe its function and effectiveness in low voltage ride through capability, this paper conducted offline simulation experiments and real-time simulation experiments. The system structure diagram is shown in Figure 3. The system simulation model is shown in Figure 4.

In off-line simulation, an average voltage converter is used in the simulation model. The simulation system consists of five doubly-fed generators and one synchronous generator.

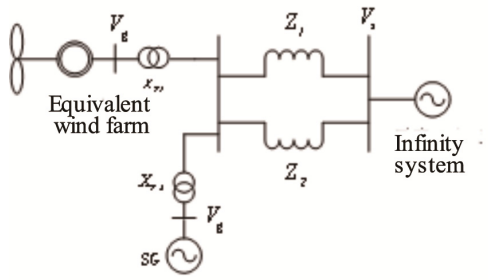

FIGURE 3. Wind-fire hybrid infinity system structure diagram.

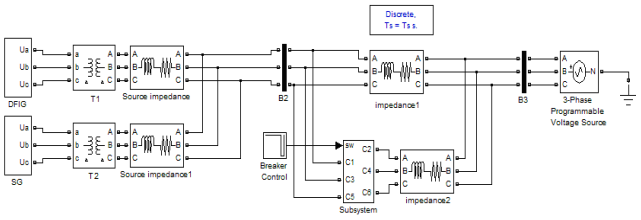

FIGURE 4. Wind-fire hybrid transmission system simulation model diagram.

The main parameters are:

Doubly-fed wind turbine parameters: rated power is $P_N = 2MW$, rated voltage is $U_N = 690V$, Rated frequency is $f_N = 50Hz$,Synchronous speed is $n_N = 1800r/min$, Stator resistance is $R_S = 0.008\Omega$, Rotor resistance is $R_r = 0.0019\Omega$ (Stator measurement), Stator inductance is $L_s = 0.002H$, $L_r = 0.0047H$(Stator measurement), Mutual sense is $L_m = 0.00547H$(Stator measurement), R=2.5kΩ.

Synchronous motor equivalent parameters: rated power is $P_N = 15MW$, Rated voltage is $U_N = 690V$, Rated frequency is $f_N = 50Hz$, Synchronous speed is $n_N = 1800r/min$, Stator resistance is $R_S = 0.00076\Omega$, Rotor resistance is $R_r = 0.000173\Omega$ (Stator measurement), Stator inductance is $L_s = 0.012H$, $L_r = 0.0047H$(Stator measurement), Mutual sense is $L_m = 0.00375H$(stator calculation value), $R = 2.5k\Omega$.

Network parameters:$X_{T1} = X_{T2} = j52.6\Omega$, $Z_1 = Z_2 = (15+j112.7)$.

Main sliding surface parameters: $k_{pq} = k_{pd} = 3.5$, $k_{iq} = k_{id} = 0.7$, $\eta_d = \eta_q = 15$, $k = 50.2$.

The simulation environment is set as follows.

When the grid fault time is t=1s, one of the two lines of the transmission line (Z_1 or Z_2) is disconnected due to the short-circuit fault trip, and the re-closing is successful when t=1.2s, and the line resumes normal power supply. The simulation results are shown in Figures 5-8.

According to the analysis of Fig. 5 and Fig. 6, the maximum common bus voltage drop value is 100V under the improved control method, while the maximum common bus voltage drop value is 500V under the traditional PI control strategy. And the output reactive power is effectively enhanced under the improved control method.

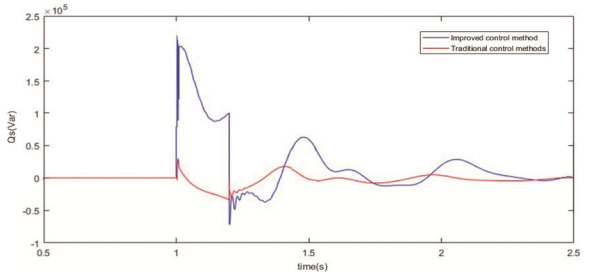

FIGURE 5. Simulation comparison of output reactive power of doubly-fed induction generator.

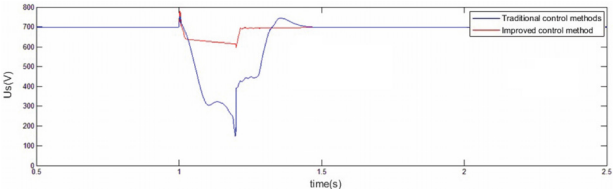

FIGURE 6. Simulation curve of voltage drop at the system common bus.

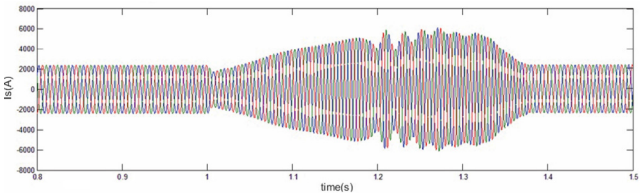

FIGURE 7. Conventional control strategy DFIG rotor current simulation curve.

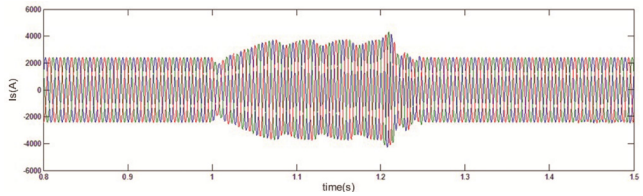

FIGURE 8. Improved control strategy DFIG rotor current simulation curve.

According to the analysis of Figure 7 and Figure 8 that with the improved control method, the maximum overcurrent of the DFIG rotor excitation current is only 4500A, but under the conventional PI excitation control, the maximum overcurrent of the DFIG rotor excitation current reaches 6500A. Therefore, when the grid voltage drops, the improved control strategy can effectively control the occurrence of rotor overcurrent.

The above is the offline simulation content of the system. The real-time simulation design of the system will be further analyzed.

Extend the single-machine control model of DFIG to the wind farm cluster control model to verify whether it is suitable for application in actual engineering. A real-time simulation system based on RTDS ''joint control of flux linkage and pitch angle'' was developed. The converter in the

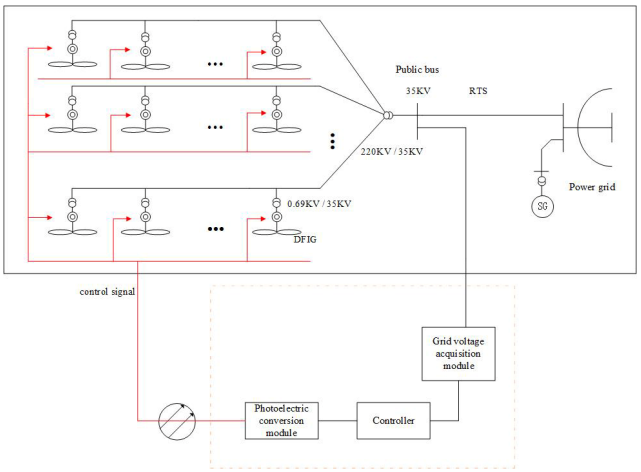

FIGURE 9. Real-time experimental system structure.

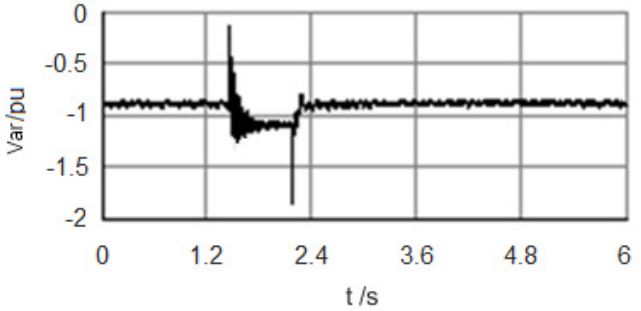

FIGURE 10. Conventional PI control doubly-fed wind turbine output reactive power response curve.

real-time simulation system uses an average voltage model. And the simulation system consists of 5 doubly-fed generators and a synchronous generator model. The wind power capacity and thermal power capacity are allocated in a ratio of 1:1.5. The real-time simulation system structure diagram is shown in Figure 9.

First, it should be noted that RTDS data acquisition is performed in a certain cycle, so it is also impossible to set the trigger time of the system failure at will. The RTDS system is connected to the control experimental device to form a closed loop control system. The transient experiment is as follows: The external grid of the experiment has a three-phase short-circuit fault at about t=1s, and the bus voltage drop fault occurs at about t=1.21s in the real-time simulation experiment.

In order to observe the control effect, the output response curves are compared according to the conventional PI control strategy and the improved control strategy adopted in this paper. RTDS is used to monitor DFIG operating conditions and common bus voltage changes in the simulated wind farm. In order to facilitate the analysis and research, this paper only monitors the working conditions of a common bus and system common bus voltage in the wind farm.

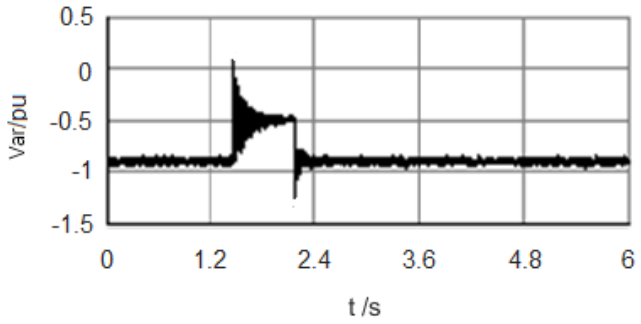

FIGURE 11. Doubly-fed wind turbine output reactive power response curve under improved control strategy.

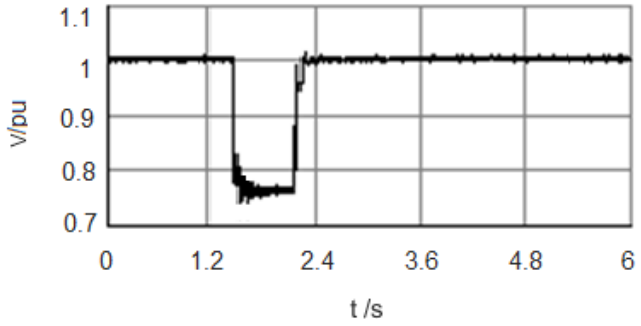

FIGURE 12. DFIG terminal voltage dip control effect curve under conventional PI control strategy.

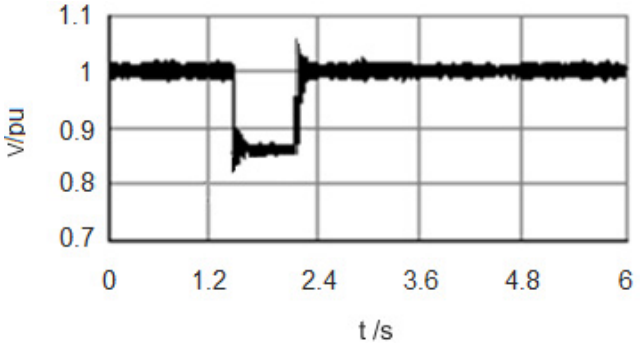

FIGURE 13. DFIG terminal voltage dip control effect curve under improved control strategy.

The reactive power variation curve of the DFIG using two control strategies is shown in Fig. 10-11. It can be seen from Fig. 9 that during the grid fault, the DFIG reactive output changes under the conventional PI control strategy is small. When using the improved control strategy of this paper, the DFIG can quickly output the output reactive power, which suppresses the system bus voltage drop.

After the wind turbine is connected to the control command issued by the upper computer, it will appropriately increase the reactive output power to suppress the common bus voltage. The common bus voltage curves are shown in Figures 12 and 13. The system bus voltage drop is 0.23 pu under the PI control method, as shown

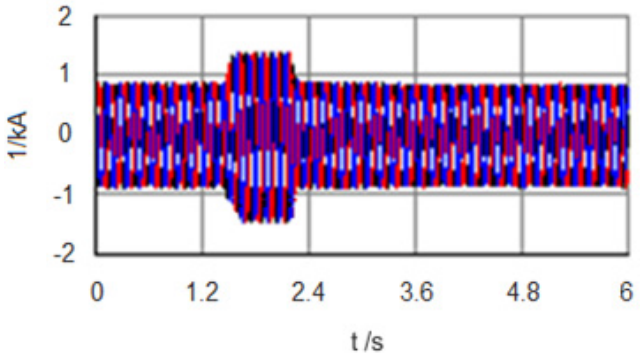

FIGURE 14. Rotor current response curve under conventional PI control strategy.

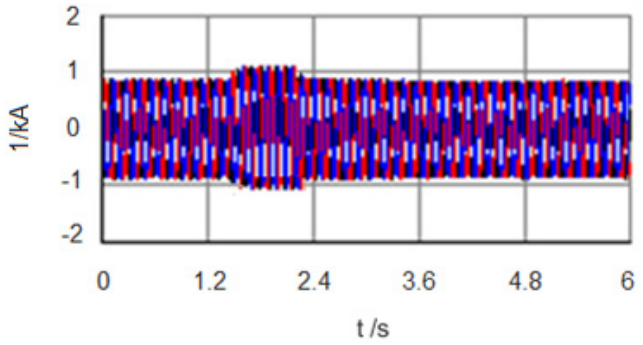

FIGURE 15. Rotor current response curve under improved control strategy.

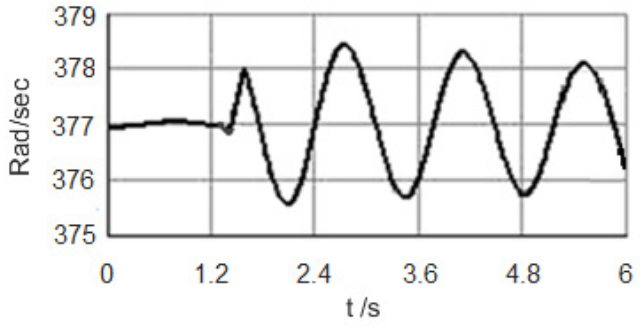

FIGURE 16. Rotor speed curve under conventional PI control strategy.

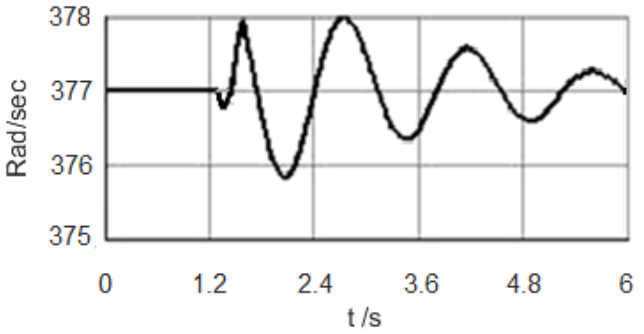

FIGURE 17. Rotor speed curve under improved control strategy.

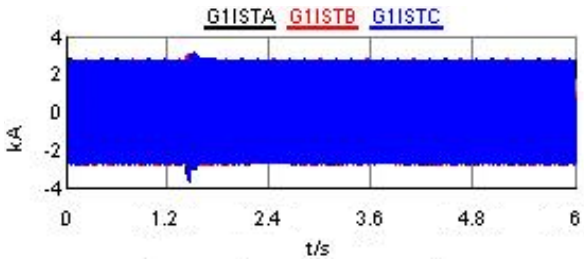

FIGURE 18. Stator current response curve under conventional PI control strategy.

FIGURE 19. Stator current response curve of improved control strategy.

in Figure 12. The system bus voltage drop is 0.15 pu under the improved control method, as shown in Figure 13.

When the grid voltage drops, the rotor current transient response curves of DFIG are shown in Figures 14 and 15. The grid voltage drop causes the DFIG rotor excitation current to increase, but the rotor excitation current has different amplitudes under the two control methods. As can be seen from Figure (14) that the excitation current of the doubly-fed wind turbine rotor increases greatly under the PI control method. The excitation current of the rotor is significantly small under the improved control method, as shown in Fig. 15.

The rotor speed variation curve is shown in Fig. 16 and Fig. 17. It can be seen from Fig. 16 that when the system fails, the sway time of the rotor speed curve in the system is longer under the conventional PI control strategy. When the improved control strategy is adopted, the doubly-fed induction generator rapidly increases the pitch angle, which increases the active output of the adjacent synchronous generator. It reduces the swing time of the synchronous generator rotor speed curve and enhances the anti-jamming capability of the system.

The stator current curve is shown in Figures 18 and 19. The "G1ISTA, G1ISTB, G1ISTC" represents the stator three-phase current. Under the improved control strategy, the stator instantaneous current will suddenly increase. However, since the stator is not directly connected to the power electronics, the instantaneous current is still within the safe range. It shows that the control strategy proposed in this paper will not have a negative impact on wind turbines and systems.

V. ANALYSIS AND DISCUSSION

In this paper, an additional control model of DFIG grid-connected rotor flux based on structure decentralization theory is proposed. In the simulation experiment, the improved

control method and PI control method proposed in this paper are compared by designing the system offline simulation experiment and the system real-time simulation experiment.

First, an off-line simulation experiment under grid faults is performed. The simulation results are shown in Figure 5-8. Under the conventional PI control strategy, the reactive power output of the wind farm has little changes, so almost no output reactive power is provided to the system; the bus voltage drop can be up to 550V, and the system dynamic recovery speed is slow; The maximum overcurrent of the DFIG rotor current reaches 6500A. Under the improved control strategy of this paper, the maximum bus voltage drop is only 100V; the maximum overcurrent of the DFIG rotor excitation current is only 4500A. The doubly-fed wind turbine can quickly output the output reactive power to suppress the system bus voltage drop.

Secondly, real-time simulation experiments were carried out when the grid was faulty. The simulation results are shown in Figure 10-19. Under the conventional PI control strategy, the system has the following characteristics: DFIG reactive power change is little; system bus voltage drop is 0.23 pu; the sway time of the synchronous generator rotor speed curve is longer in the system; the excitation current of the doubly-fed wind turbine increases greatly. Under the improved control strategy of this paper, the system features are as follows: the doubly-fed wind turbine can quickly increase the reactive power to suppress the system bus voltage drop; the system bus voltage drop is 0.15 pu; it reduces the sway time of the synchronous generator rotor speed curve; the excitation current of the doubly-fed wind turbine increases significantly.

In summary, the real-time simulation experiment results are consistent with the offline simulation results. Using the improved control method, it can effectively reduce the drop of the bus voltage and increase the dynamic recovery capability of the system. It can also effectively suppress the overcurrent of the rotor and enhance the anti-interference ability of the system. This control strategy improves the low voltage ride through capability to some extent.

VI. CONCLUSION

In this paper, an adaptive terminal sliding mode additional control strategy for doubly-fed wind farm rotor flux is proposed to improve low voltage ride through capability of wind-fire hybrid transmission system, taking grid-connected doubly-fed wind farm as the research object. On the one hand, the control strategy improves the low voltage ride-through capability of the doubly-fed wind farm when the grid voltage drops. On the other hand, it effectively suppresses sudden changes in the common bus voltage of the dual power supply. The simulation results show that the bus voltage drop is reduced by 450V, and the rotor current overcurrent maximum is reduced by 2000A comparing with the traditional PI control method, under offline simulation. The system bus voltage drop value was reduced by 0.08 pu under real-time simulation. Therefore, during the power failure, the wind farm can quickly generate reactive power under the improved control method, which can effectively suppress the voltage drop of the common bus. To sum up, it can improve the low voltage ride through ability to some extent.

REFERENCES

[1] O. Noureldeen and I. Hamdan, "A novel controllable crowbar based on fault type protection technique for DFIG wind energy conversion system using adaptive neuro-fuzzy inference system," *Protection Control Mod. Power Syst.*, vol. 3, no. 1, p. 35, 2018.

[2] S. Luo and L. Zhu, "Research on control strategy of double feed converter under grid voltage soared," *Power Syst. Protection Control*, vol. 45, no. 24, pp. 123–129, Dec. 2017.

[3] Y. E. Yanfei, W. Qi, and C. Ning, "Wind forecast model considering the characteristics of temporal and spatial distribution," *Power Syst. Protection Control*, vol. 45, no. 4, pp. 115–119, 2017.

[4] M. Alsumiri, L. Li, L. Jiang, and W. Tang, "Residue Theorem based soft sliding mode control for wind power generation systems," *Protection Control Mod. Power Syst.*, vol. 3, no. 1, 2018, Art. no. 24.

[5] S. Boubzizi, H. Abid, A. El Hajjaji, and M. Chaabane, "Comparative study of three types of controllers for DFIG in wind energy conversion system," *Protection Control Mod. Power Syst.*, vol. 3, no. 1, p. 21, 2018.

[6] W. Tang, J. Hu, F. Liu, and Y. Chang, "Modeling of DFIG-based wind turbine for power system transient response analysis in rotor speed control timescale," *IEEE Trans. Power Syst.*, vol. 33, no. 6, pp. 6795–6805, Nov. 2018.

[7] J. Li, K. Jiang, G. Liu, X. Zeng, M. Yu, and J. Yao, "High voltage ride-through control strategy of doubly-fed induction generator based wind turbines with a series grid-side converter," *Power Syst. Technol.*, vol. 38, no. 11, pp. 3037–3044, Nov. 2014.

[8] F. E. V. Taveiros, L. S. Barros, and F. B. Costa, "Heightened state-feedback predictive control for DFIG-based wind turbines to enhance its LVRT performance," *Int. J. Electr. Power Energy Syst.*, vol. 104, pp. 943–956, Jan. 2019.

[9] R. Fang, W. Chen, D. Xu, and X. Zhang, "Improved virtual inductance based control strategy of DFIG under weak grid condition," in *Proc. IEEE Int. Power Electron. Conf. (IPEC-Niigata-ECCE Asia)*, May 2018, pp. 4213–4219.

[10] K. Givaki, D. Chen, and L. Xu, "Current error based compensations for VSC current control in weak grids for wind farm applications," *IEEE Trans. Sustain. Energy*, vol. 10, no. 1, pp. 26–35, Jan. 2019.

[11] S. Lu, Z. Xu, L. Xiao, W. Jiang, and X. Bie, "Evaluation and enhancement of control strategies for VSC stations under weak grid strengths," *IEEE Trans. Power Syst.*, vol. 33, no. 2, pp. 1836–1847, Mar. 2018.

[12] M. Kuzhali, S. J. Isac, and S. Poongothai, "Improvement of low voltage ride through capability of grid-connected DFIG WTs using fuzzy logic controller," in *Proc. Int. Conf. Intell. Comput. Appl.* Singapore: Springer, 2019, pp. 349–359.

[13] Y. M. Alsmadi, L. Xu, A. J. P. Ortega, A. Y. Abdelaziz, A. Wang, Z. Albataineh, and F. Blaabjerg, "Detailed investigation and performance improvement of the dynamic behavior of grid-connected DFIG-based wind turbines under LVRT conditions," *IEEE Trans. Ind. Appl.*, vol. 54, no. 5, pp. 4795–4812, Sep./Oct. 2018.

[14] S. G. Vennelaganti and N. R. Chaudhuri, "New insights into coupled frequency dynamics of AC grids in rectifier and inverter sides of LCC-HVDC interfacing DFIG-based wind farms," *IEEE Trans. Power Del.*, vol. 33, no. 4, pp. 1765–1776, Aug. 2018.

[15] S. Ghosh and S. Kamalasadan, "An energy function-based optimal control strategy for output stabilization of integrated DFIG-flywheel energy storage system," *IEEE Trans. Smart Grid*, vol. 8, no. 4, pp. 1922–1931, Jul. 2017.

[16] M. K. Döşoğlu, "Enhancement of SDRU and RCC for low voltage ride through capability in DFIG based wind farm," *Elect. Eng.*, vol. 99, pp. 673–683, Jun. 2017.

[17] W. Li, G. Joos, and J. Belanger, "Real-time simulation of a wind turbine generator coupled with a battery supercapacitor energy storage system," *IEEE Trans. Ind. Electron.*, vol. 57, no. 4, pp. 1137–1145, Apr. 2010.

[18] M. K. Döşoğlu, "A new approach for low voltage ride through capability in DFIG based wind farm," *Int. J. Elect. Power Energy Syst.*, vol. 83, pp. 251–258, Dec. 2016.

[19] M. Kalantar, "Dynamic behavior of a stand-alone hybrid power generation system of wind turbine, microturbine, solar array and battery storage," *Appl. Energy*, vol. 87, no. 10, pp. 3051–3064, 2010.

[20] M. K. Döşoğlu, "Nonlinear dynamic modeling for fault ride-through capability of DFIG-based wind farm," *Nonlinear Dyn.*, vol. 89, no. 4, pp. 2683–2694, Sep. 2017.
[21] M. Rahimi and M. Parniani, "Coordinated control approaches for low-voltage ride-through enhancement in wind turbines with doubly fed induction generators," *IEEE Trans. Energy Convers.*, vol. 25, no. 3, pp. 873–883, Sep. 2010.
[22] M. K. Döşoğlu, "Hybrid low voltage ride through enhancement for transient stability capability in wind farms," *Int. J. Electr. Power Energy Syst.*, vol. 78, pp. 655–662, Jun. 2016.
[23] M. Rahimi and M. Parniani, "Low voltage ride-through capability improvement of DFIG-based wind turbines under unbalanced voltage dips," *Int. J. Electr. Power Energy Syst.*, vol. 60, pp. 82–95, Sep. 2014.
[24] B. Kai, S. Peng, X. Hailiang, L. Hanmin, L. Jingbo, and Z. Yangfan, "A high voltage ride-though control strategy for DFIG-based wind turbines," *Renew. Energy Resour.*, vol. 34, no. 1, pp. 21–29, Jan. 2016.
[25] J. Yao, L. Guo, X. Zeng, Y. Tan, and X. Yin, "Research on HVRT control of DFIG system based on series grid-side converter during asymmetrical grid voltage swell," *Power Syst. Technol.*, vol. 40, no. 7, pp. 2067–2074, Jul. 2016.
[26] Y. Zhang, Q. Li, S. Qin, and J. Zhang, "Wind farm HVRT capability improvement based on coordinated reactive power control strategy," *J. Eng.*, vol. 2017, no. 13, pp. 756–761, 2017.
[27] X. Ma and H. Yang, "IMC robust control for high-voltage ride-through of doubly fed induction wind generator," *IEEJ Trans. Elect. Electron. Eng.*, vol. 13, no. 9, pp. 1265–1275, 2018.
[28] L. Dai, S. Qin, R. Wang, S. Li, and C. Chen, "Research and experiment on high voltage ride through for direct-drive PMSG-based wind turbines," *Power Syst. Technol.*, vol. 42, no. 1, pp. 147–153, 2018.
[29] X.-Y. Xiao, R.-H. Yang, Z.-X. Zheng, and X.-Y. Chen, "Integrated DFIG protection with a modified SMES-FCL under symmetrical and asymmetrical faults," *IEEE Trans. Appl. Supercond.*, vol. 28, no. 4, Jun. 2018, Art. no. 5400606.
[30] H. Xu, W. Zhang, J. Chen, D. Sun, and Y. He, "A high-voltage ride-through control strategy for DFIG based wind turbines considering dynamic reactive power support," *Proc. CSEE*, vol. 33, no. 36, pp. 112–119, 2013.
[31] B. Yang, T. Yu, H. Shu, J. Dong, and L. Jiang, "Robust sliding-mode control of wind energy conversion systems for optimal power extraction via nonlinear perturbation observers," *Appl. Energy*, vol. 210, pp. 711–723, Jan. 2018.
[32] F. Golnary and H. Moradi, "Design and comparison of quasi continuous sliding mode control with feedback linearization for a large scale wind turbine with wind speed estimation," *Renew. Energy*, vol. 127, pp. 495–508, Nov. 2018.

XINYU LIU was born in Henan, China, in 1976. He received the master's and Ph.D. degrees from Zhengzhou University, China.

Since 2004, he has been with the North China University of Water Resources and Electric Power, where he is currently an Associate Professor and a Master Tutor. He is the author of two books. He received the third prize of Henan Science and Technology Progress Award and the second prize of Henan Province Information Technology Education Outstanding Achievement Award. In 2016, he was named "Young backbone teacher of Henan colleges and universities".

GUOFANG WU was born in April 1994. He is currently pursuing the master's degree with the North China University of Water Resources and Electric Power. His main research interests include research on joint optimization controller for grid-connected high and low voltage crossing of large-scale doubly-fed wind farms.

XIANWEI LI was born in September 1994. He is currently pursuing the master's degree with the North China University of Water Resources and Electric Power. His main research interest includes the control strategy of converters with double-fed wind power grid-connected.